

Kinetic processes in Ar-Kr-F₂ laser mixtures

W. L. Morgan and A. Szöke

University of California, Lawrence Livermore National Laboratory, Livermore, California 94550

(Received 27 August 1980)

Time-dependent fluorescence measurements were made on Ar-F₂, Kr-F₂, and Ar-Kr-F₂ mixtures excited by a short-pulse, low-current electron beam excitation in pressure ranges appropriate for rare-gas-halide lasers. A kinetic model was assembled that correctly analyzes integrated intensities and time dependences of the various emission bands of ArF*, Ar₂F*, KrF*, and Kr₂F*. We present the structure of the model and several revised rate coefficients obtained from it. The model also fits other published experimental data and agrees well with KrF laser pulse shapes and efficiencies. Cross sections for electron-impact dissociative excitation of F₂, which were obtained from analysis of published data, are also presented.

I. INTRODUCTION

Because the krypton-fluoride laser is the most efficient high-power short-wavelength laser available, there has been much effort devoted to understanding the formation and quenching kinetics of this excimer. The kinetics of KrF* and Kr₂F* are well understood now although the rates of certain processes, such as B-C state mixing and electron quenching, are not accurately known. The rare-gas-fluoride kinetic scheme has been discussed in great detail in the literature.^{1,2,3} Briefly, it involves production of excited rare-gas atoms, rare-gas ions, and F⁻ negative ions by the electron beam. In one mechanism this is followed by recombination of the positive and negative ions to form an excited rare-gas-fluoride molecule (exciplex). At pressures greater than about one atmosphere the positive ions are primarily dimers. The exciplexes so produced then either radiate or are quenched by one of a variety of processes. Three-body quenching by rare-gas atoms produces the R₂F* trimers. In addition to the ionic channel just described the rare-gas-fluoride exciplex may also be formed by the so-called "harpoon" reaction between an excited rare-gas atom and an F₂ molecule. This neutral channel is thought to be more important in a discharge laser than it is in an electron-beam pumped laser.³

In an effort to assemble a kinetic model for Ar-Kr-F₂ mixtures, in order to investigate scaling of the KrF* laser for laser fusion applications, we have performed kinetics experiments on Ar-F₂, Kr-F₂, and Ar-Kr-F₂ mixtures. A short-pulse, low-current *e*-beam was used to excite the rare-gas-halogen mixture. Time-dependent experimental fluorescence data were collected at various wavelengths, pressures, and concentration ratios. The kinetic model was used to fit these results both in integrated (relative) intensity and in its time dependence. A few of the

kinetic constants were varied to get a best fit to the experiments thereby constructing a self-consistent set of kinetic data. Calculations were then performed to model experiments appearing in the published literature. The model was found to give good agreement with these data as well. With such a kinetic model we may explore the parameter space of operation for a KrF* laser with respect to gain, loss, and efficiency in terms of Ar-Kr-F₂ partial fractions, total pressure, gas temperature, and *e*-beam power deposition and pulse length.

II. EXPERIMENTAL

Mixtures of the noble gases, argon, krypton, and fluorine at total pressures of 250–2000 Torr were excited by an electron beam of short duration, and their fluorescent spectra were studied with time and spectral resolution. A block diagram of the apparatus is shown in Fig. 1. The electron gun has 80 keV of energy and provides a pulse of electrons of 24-nsec duration, with rise and fall times of 1 nsec. The current density at the foil is approximately 0.15 A/cm². The pulse repetition rate is variable up to 50 pulses

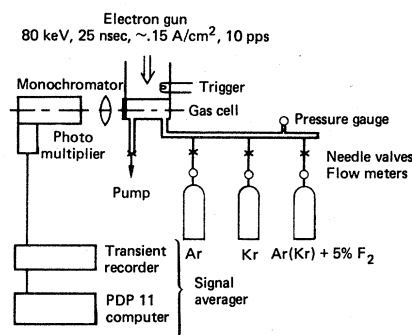


FIG. 1. Schematic of experimental apparatus.

per second, but was run typically at 10 pps. The electron beam enters the cell through a narrow 0.5 mm × 3 cm slit covered with a 2.5 micron-thick foil. We did not attempt to correct for the divergence of the electron beam in our results. The gases were slowly flown through our cell, typically at 100 standard cm³/minute speed.

The gases were flown through individual flow meters, their concentrations being taken as the ratios of their mass flows. Every concentration and pressure was flown for at least one hour prior to taking measurements in order to establish equilibrium. We found experimentally that at fixed concentration ratios and varying pressures the gases reach equilibrium faster than vice versa but, in any case, we always waited long enough that the results did not change during any given run. The fluorescent signal was viewed through LiF lenses and a 300-mm monochromator, detected with a photomultiplier (GaAs photosurface), recorded on a transient recorder, and averaged on a minicomputer. It was found experimentally that the total time resolution of the system was better than 5 nsec. The signal was averaged between 100 and 400 times, depending on the signal strength. The computer also calculated the logarithm of the signal, displayed it, and fitted a straight line (weighted by the signal strength) in an interval selected by the operator. In this way the decay times were found. The integrated signal was obtained electronically with an RC integrator, and averaged by photographing the face of an oscilloscope. It should be pointed out that the computer models were fitted to the whole fluorescence curve, not only to its decay. In particular, the parameters are integrated intensity, peak intensity, delay of the peak intensity, decay rates, and deviations from exponential decay.

Research grade Ar and Kr were used without further purification. Fluorine was first diluted

to 5% with Ar (or Kr) in a bottle, and this gas mixture was used for flow.

In our experiments we used binary mixtures of Ar-F₂ and Kr-F₂, and ternary Ar-Kr-F₂ mixtures. In the binary mixtures the total pressures of 250, 500, 1000, 1950 Torr, and F₂ concentrations of 0.035, 0.1, and 0.3% were systematically explored. In Ar-Kr-F₂ mixtures several "cuts" were made with concentrations of Kr and F₂ in the 0.3–3% and 0.035–0.3% range, respectively, but not all combinations were measured.

Emissions were measured on the peaks of ArF* (*B-X*) at 193 nm (the apparent red shift from 193 nm was caused by the falling sensitivity of the photomultiplier) and on the Ar₂F* band at 295 nm. In KrF* all three bands were monitored: the *D-X* at 221 nm, the *B-X* at 249 nm, and the *C-A* band at 280 nm. Also Kr₂F* emission at 380 nm, and the Kr [4p' ($\frac{1}{2}$) J=1 - 4s' ($\frac{1}{2}$)^o J=0] line was monitored at 772.4 nm. In ternary mixtures there is an overlap between the Ar₂F* and KrF* (*C-A*) emission such that their intensities can not always be separately measured.

Sample spectra are shown in Fig. 2, for 1000-Torr Ar and 0.1% F₂, together with the results of our computer model. The spectra in these cases were averaged 100 times. The slits were always adjusted so that the maximum photomultiplier output did not exceed 300 mV. The time dependences of these spectra are typical: The ArF* emission "integrates" the *e*-beam pulse and starts to decay immediately, in an exponential way, and later in a way that is slower than exponential (more like 1/*t*). The Ar₂F* emission peaks with a delay and becomes very nearly exponential at later times.

It should be pointed out that the dependence of any given band intensity on the various gas pressures can be found this way reliably. We did not attempt to establish the relative intensities of various bands.

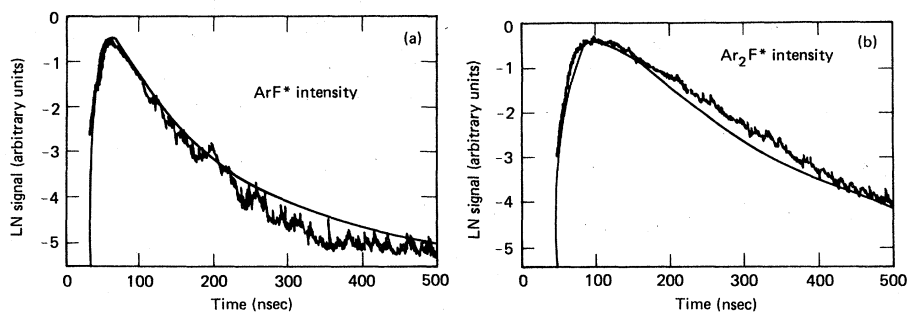


FIG. 2. Comparison of measured and calculated time dependence of fluorescent intensity for 1000-Torr Ar and 1-Torr F₂; (a) ArF* fluorescence, (b) Ar₂F* fluorescence.

III. MODEL

A. General description

The kinetic model used in this analysis includes electron-impact collisions, heavy-particle kinetics, and photon processes.

The computer program is constructed to read in symbolic chemical reactions, rate coefficient data, and electron-impact data. The rate coefficients are given as functions of the gas and electron temperatures. The computer constructs the appropriate rate equations for the various chemical species and solves for the time-dependent populations, using a special integrator for stiff problems. By extensive use of computer graphics, the program can quickly determine decay rates and integrated intensities for comparison with experimental data.

Electrons are taken to be of two kinds: high-

energy beam electrons and low-energy electrons. The beam electrons cause excitations and ionizations the rates of which are the result of a high-energy electron slowing down calculation. This process eventually results in slow electrons. All slow electrons produced are assumed to have a Maxwell-Boltzman energy distribution. The electron temperature and gas temperature are calculated as a function of time using energy balance in all kinetic processes.

B. Electron impact processes

1. Discrete slowing down calculation

Using the high-energy electron-impact cross sections referenced in Table I, a discrete electron slowing calculation^{17,18,19} is performed. In this calculation a high-energy electron is slowed down by collisions and a record is kept of the

TABLE I. References for electron-impact cross-section data.

Electron-impact process	References	Remarks
1. Momentum transfer-Ar	4	
2. Ar → Ar(³ P ₀ + ³ P ₂)	5, 6	Ar*
3. Ar → Ar(³ P ₁)	5, 6	Ar*
4. Ar → Ar(¹ P ₁)	5, 6	Ar*
5. Ar → Ar(4p)	5, 6	Ar**
6. Ar → Ar ⁺	7	
7. Ar ⁺ → Ar**	8	K (4s → 4p) cross section
8. Ar* → Ar ⁺	9	
9. Ar** → Ar ⁺		Scaling of cross section (8)
10. Momentum transfer-Kr	4	
11. Kr → Kr*	5	Total excitation cross section including Kr (5p)
12. Kr → Kr ⁺	7	
13. Kr* → Kr**	10	Rb (5s → 5p) cross section
14. Kr* → Kr ⁺	9	
15. Kr** → Kr ⁺		Scaling of cross section (14)
16. Momentum transfer-F ₂	11, 12	Apparent resonance not included (12)
17. F ₂ vibrational excitation	13	
18. F ₂ → F + F ⁻	14	
19. F ₂ (X) → F ₂ (³ Π _u) → 2F	15	See text
20. F ₂ (X) → F ₂ (¹ Π _u) → 2F	16	See text
21. F ₂ (X) → F ₂ * → 2F	16	

number of excitations and ionizations that occur. The secondary electrons resulting from ionization by a primary of energy E_p are produced with a distribution of energy E_s given by the differential ionization cross section $d\sigma(E_p, E_s)/dE_s$. These secondaries are in turn slowed down and the number of excitations and ionizations recorded. This calculational procedure is continued until all electrons have been slowed to some minimum energy. This calculation provides the total number of excitations N_j to each state j , the energy loss per electron-ion pair, the total number of secondaries produced, and a secondary electron energy spectrum (electrons/eV) for electrons between $E = 0$ and $E = E_{\min}$. As defined by Peterson and Allen²⁰ the excitation efficiency for each state j is

$$\epsilon_j \equiv \frac{W_j N_j}{E_p},$$

where W_j is the excitation energy of state j . They have pointed out that for E_p sufficiently large, above 500–1000 eV, the ϵ_j are constant for all E_p . This is because the high-energy tails of all allowed electron-impact cross sections have the same energy dependence. In these calculations we took $E_p = 1000$ eV and $E_{\min} = 15.8$ eV, the ionization energy of argon. This provides a source of low-energy, 0–15.8 eV, electrons. If P_{eb} is the electron beam power deposition rate per unit volume, the rate of excitation of state j due to the e beam is equal to $P_{eb}\epsilon_j/W_j$. The rate of heating of the free electrons is then $P_{eb}(1 - \sum_{\text{all } j} \epsilon_j)$.

2. F₂ cross sections

Substantial effort was involved in assembling the set of F₂ electron-impact cross sections. For dissociative attachment of F₂ we used the cross section measured by Chanry.¹⁴ This cross section, as discussed in the review by Nygaard *et al.*²¹ gives attachment rates that agree well with experiment over a wide range of electron temperature.

Because the low-lying excited states of F₂ have repulsive potential curves, low-energy electrons that do not dissociatively attach or vibrationally excite F₂ are expected to dissociate the molecule. This destruction of F₂ by electron-impact dissociation has been shown by Nighan^{22,23} to be responsible for instability in a KrF discharge. This process may also have a deleterious effect on the performance of e -beam pumped lasers. There have been two experiments reported on that have yielded data related to F₂ dissociation. Electron beam experiments of Wilson *et al.*²⁴ have shown that approximately three F

atoms are produced for each electron molecule ionizing collision. This gives an energy loss of about 12 eV for each F atom produced assuming an energy loss of 35 eV per electron-ion pair. Using an e beam sustained N₂-F₂ discharge, Chen *et al.*²⁵ measured a sustainer enhancement factor for the production of F atoms as a function of applied electric field. This enhancement factor is defined as the rate of F atom production by e beam plus sustainer divided by the production rate due to the e beam alone.

We are able to perform calculations simulating these experiments using the electron slowing down code described above for the Wilson *et al.*²⁴ experiment and using a Boltzmann code for the Chen *et al.*²⁵ experiment. The Boltzmann code²⁶ solves the time-dependent Boltzmann equation for a discharge including momentum transfer, inelastic, superelastic, dissociative attachment, and electron-electron collisions. Included also is the source function arising from the electron slowing calculation. In these calculations we used Chanry's¹⁴ F₂ dissociative attachment cross section, Hall's¹³ F₂ vibrational excitation cross sections, the Born cross sections of Rescigno *et al.*¹⁶ for the allowed F₂ electronic transitions, and the distorted wave cross sections of Fliflet *et al.*¹⁵ (shown in Fig. 3) for exchange excitation of the 3.35-eV F₂(³Π_u) state. The cross sections for excitation to F₂(³Π_u) and F₂(¹Σ_u) were parametrized using an analytic expression²⁷ and then adjusted to give best agreement between the calculations and the experimental data. The calculations performed using

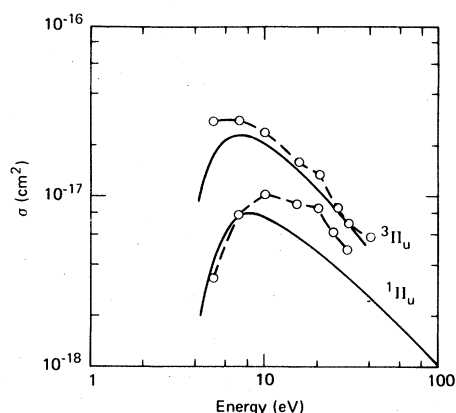


FIG. 3. Electron-impact excitation cross sections for F₂. Dashed curves: calculations by Fliflet *et al.*¹⁵ for excitation of F₂(³Π_u) without target polarization effects (upper curve) and with polarization effects (lower curve). Solid curves: cross sections for excitation of F₂(³Π_u) (upper curve) and F₂(¹Π_u) (lower curve) derived from analysis of experimental data as described in the text.

the F_2 cross sections shown by the solid lines in Fig. 3 yielded sustainer enhancement factors in good agreement with the Chen *et al.*²⁵ data. For the conditions of the Wilson *et al.*²⁴ experiment the calculations gave a 32.4 eV energy loss per electron-ion pair for electrons in F_2 , a 10.8-eV energy loss per F atom, and an F-atom production rate of 3.0 per ionizing collision.

C. Heavy particle kinetics

In our work we concentrated on the detailed understanding of the formation kinetics, leaving most of the destruction rates unchanged. The basic formation and quenching kinetics of ArF^* and KrF^* in electron-beam pumped Ar-Kr- F_2 mixtures has been described by Rokni *et al.*¹ The most important reactions and rate coefficients are shown in Table II. We discuss below the treatment of some of the important rate processes

as well as some of the limitations of our model.

In our *e*-beam experiment operating at gas pressures of greater than 500 Torr the primary rare-gas halide (RGH) formation process is positive-negative ionic recombination. Little experimental data exists at all for positive-negative ion recombination rates and none at high pressure where the effective two-body rate is determined by the rate of diffusion of the ions toward each other in the background gas. A theoretical description of this process was given by Bates and Flannery³⁴ and has been recently modified by Flannery.³⁵ Flannery and Yang³⁴ have computed recombination rates for the rare-gas atomic and dimer ions with F^- in rare-gas buffers. We have used in our model the Flannery and Yang³⁶ formula to calculate the ionic recombination rates. The mobilities of the positive and negative ions in the buffer gas are used in the formula to calculate the effective two-body rate for the molecular recom-

TABLE II. Reactions and rate coefficient data for Ar-Kr- F_2 kinetics.

Reaction	Rate coefficient	
	This work	Literature
$Ar^+ + 2Ar \rightarrow Ar^+ + Ar$		2.5×10^{-31} (Ref. 28)
$Kr^+ + 2Kr \rightarrow Kr_2^+ + Kr$		2.5×10^{-31} (Ref. 28)
$Kr^+ + Kr + Ar \rightarrow Kr_2^+ + Ar$		2.5×10^{-31} (estimate)
$Kr^+ + 2Ar \rightarrow ArKr^+ + Ar$		1.0×10^{-31} (estimate)
$Ar_2^+ + F^- + Ar \rightarrow ArF^* + 2Ar$	0.3 FY ^a	FY
$ArF^* + 2Ar \rightarrow Ar_2F^* + Ar$	2.0×10^{-31}	4.0×10^{-31} (Ref. 29)
$Ar_2F^* + F_2 \rightarrow PROD$	4.0×10^{-10}	2.1×10^{-10} (Ref. 39)
$Ar_2F^* + Ar \rightarrow PROD$	1.2×10^{-13}	
$Kr^+ + F^- + Kr \rightarrow KrF^* + Kr$	0.25 FY	FY
$Kr_2^+ + F^- + Kr \rightarrow KrF^* + 2Kr$	0.25 FY	FY
$KrF^* + 2Kr \rightarrow Kr_2F^* + Kr$	1.0×10^{-31}	$(2.9-9.7) \times 10^{-31}$ (Ref. 29)
$Kr_2F^* + F_2 \rightarrow PROD$	1.5×10^{-10}	4.3×10^{-10} (Ref. 30)
$Ar^* + F_2 \rightarrow ArF^* + F$	4.0×10^{-10}	$(4.0-10.0) \times 10^{-10}$ (Ref. 31-33)
$ArF^* + Kr \rightarrow KrF^* + Ar$	3.0×10^{-10}	1.6×10^{-9} (Ref. 1)
$KrF^* + 2Ar \rightarrow ArKrF^* + Ar$	4.0×10^{-32}	7.0×10^{-32} (Ref. 29)
$ArKrF^* + Kr \rightarrow Kr_2F^* + Ar$	6.0×10^{-11}	
$KrF^* + Kr + Ar \rightarrow Kr_2F^* + Ar$	8.0×10^{-31}	6.5×10^{-31} (Ref. 29)
$Ar_2^+ + Kr \rightarrow Kr^+ + 2Ar$	7.5×10^{-10}	7.5×10^{-10} (Ref. 28)
$Kr_2^+ + F^- + Ar \rightarrow KrF^* + Kr + Ar$	0.7 FY	FY
$ArKr^+ + Kr \rightarrow Kr_2^+ + Ar$	1.0×10^{-10}	3.2×10^{-10} (Ref. 28)
$ArKr^+ + F^- + Ar \rightarrow KrF^* + 2Ar$	0.5 BF ^b	BF

^a FY: calculations of Flannery and Yang, Ref. 36.

^b BF: theory of Bates and Flannery, Ref. 34.

bination process. This allows the code to evaluate the rate coefficient for any pressure and temperature.

In our model we have assumed KrF* to be a single species even though it really consists of two states, KrF*(B²Σ) and KrF*(C²Σ). The states are nearly degenerate, the estimated separation being approximately 0.08 eV, with the B state calculated to lie lower in energy although there is experimental evidence that the C state may lie lower. In using a single KrF* state we are assuming that the B and C states are statistically mixed by collisions on time scales short compared to the other important kinetic processes involving KrF*. There is some experimental evidence to support this assumption.³⁷

IV. RESULTS OF EXPERIMENTS AND MODELING

The experiments were performed systematically on Ar-F₂, Kr-F₂, and Ar-Kr-F₂ mixtures. Decay rates, integrated intensities, and delay times of peak fluorescence were measured for the diatomic and triatomic RGH exciplexes. Using the model, key rate coefficients can be determined by varying systematically those rates that influence the results most and that were judged to be most important or most in doubt, until good agreement between calculation and experiment was obtained. This always involves a great amount of judgment, therefore the fitting procedure will be described in the following in detail.

A. Ar-F₂ and Kr-F₂ kinetics

Figure 4 shows the decay rates of ArF* fluorescence as a function of F₂ percentage and parametric in total pressure. The decay rate is measured during the period immediately following

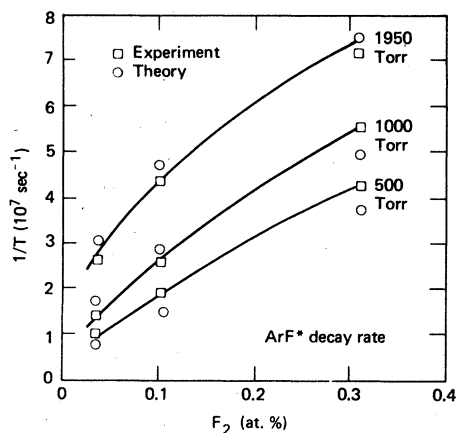


FIG. 4. ArF* fluorescence decay rates as a function of F₂ percentage and parametric in total gas pressure of Ar-F₂ mixture.

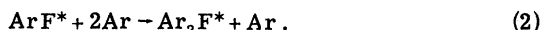
e beam termination. The kinetic chain for formation of ArF* is these experiments, even at 500-Torr total pressure, consists of rapid Ar₂⁺ dimer ion formation from Ar⁺ and subsequent recombination with F⁻ to form ArF*. Due to its very short radiative lifetime [4 nsec (Ref. 38)], the apparent decay rate of ArF* in the afterglow is a measure of its formation rate. Flannery and Yang find the effective two-body rate for ionic recombination



to increase linearly with pressure at pressures of less than about one-half atmosphere. At higher total pressure the rate becomes diffusion limited with a peak value of 3.1×10^{-6} cm³-sec at 1.6 atm. We fitted the results by scaling these calculations with a constant scale factor for all pressures although, in reality, it probably is a function of pressure. In the model calculations, compared with experiment in Fig. 4, it was found that a recombination rate coefficient of $\frac{1}{3}$ the Flannery and Yang value gives the best results.

Due to the low electron beam current density the electron density in the plasma is in the range 10^{12} – 10^{13} cm⁻³ during the pulse. It of course vanishes very rapidly in the afterglow due to F₂ dissociative attachment. Because there are no electrons in the afterglow, electron quenching of the excimer is negligible and dissociative recombination of the dimer ion is not competitive with ion-ion recombination. Due to the weak excitation, the myriad other excited state-excited state collisional processes may be neglected also. Additionally, effects due to F₂ burnout and subsequent gas heating are minimized.

The integrated intensity of ArF*, as a function of pressure, is sensitive to the rate of



This is the primary Ar₂F* formation process. Because the stable configuration of Ar₂F* is triangular, the probability of its being formed directly by ionic recombination is small. The rate coefficient for three-body formation of Ar₂F* from analysis of ArF* integrated intensity is 2×10^{-31} cm⁶/sec. The decay rate of Ar₂F* as a function of total pressure and parametric in F₂ fraction is shown in Fig. 5. Due to the long ArF₂* radiative lifetime (185 nsec) the loss of Ar₂F* is due primarily to quenching by molecular fluorine. The slopes of the solid lines in Fig. 5 that fit the experimental data quite well give an apparent rate of 2×10^{-10} cm³/sec for F₂ quenching. In fact the solid lines were calculated by the model using a value of 4×10^{-10} cm³/sec. This anomaly appears because we are not looking at a purely

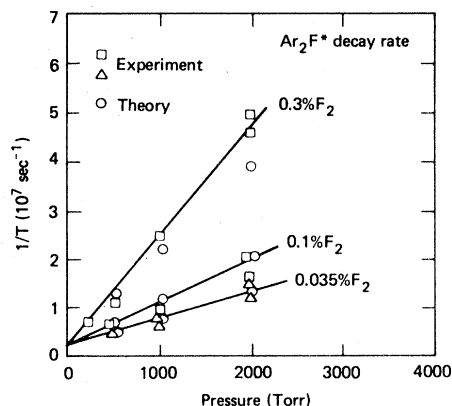
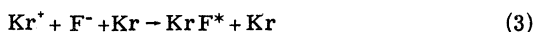


FIG. 5. Ar_2F^* fluorescence decay rates as in Fig. 4.

decaying system: the formation rate Ar_2F^* is not negligible with respect to the destruction rate. For the same reason the extrapolated zero pressure intercept does not give the correct radiative lifetime (which was actually used in the model).

Another comparison of experimental data and model calculation is shown in Fig. 2(b). Here the two curves are normalized in peak amplitude only. Note that the predicted delay time to peak fluorescence is in excellent agreement with the experimental value. For small current densities, such as in this experiment, the delay time is sensitive to e -beam current, decreasing as current increases. This is a result of electron-impact dissociative attachment of F_2 being the rate limiting step in the chain of reactions leading to Ar_2F^* .

We followed the same procedure to analyze the Kr- F_2 mixtures. As one might expect, the kinetics of Kr- F_2 mixtures is nearly identical to that of Ar- F_2 mixtures. In Kr- F_2 , in contrast to Ar- F_2 , the reaction



is the primary KrF^* formation process at 500 Torr. We find the rates for both this and the dimer-ion recombination reaction to be $\frac{1}{4}$ the theoretical Flannery and Yang rates.

As in the Ar- F_2 mixture we were able to deduce Kr_2F^* formation and quenching rates, which are shown in Table II.

In summary, for the binary rare-gas-halogen mixtures we have been able to estimate kinetic rate coefficients by systematic modeling of experimental fluorescence data. We start the analysis procedure by studying the decay rates of the diatomic RGH molecules. These, as discussed above, reflect the formation rate of the ArF^* or KrF^* . Analysis of the pressure dependence of the integrated RGH fluorescent intensity provides the three-body quenching rate of ArF^*

or KrF^* . This is also the formation rate of the triatomic species, Ar_2F^* or Kr_2F^* . The decay rates and integrated fluorescence intensities of the triatomics then provide information on the quenching of these species.

We will now discuss the extension of this approach to study of mixtures, which are used in krypton-fluoride lasers.

B. Ar-Kr- F_2 mixtures

The kinetics of the Ar-Kr- F_2 mixture is much more complicated than the kinetics of the binary mixtures. A schematic diagram of the kinetic chain is shown in Fig. 6. There are clearly many different channels, ionic and neutral, to form KrF^* through the argon and krypton species. Which ones are dominant depends upon the total pressure and the fractions of Ar, Kr, and F_2 . By performing the experiments over a wide range of values of these variables we have been able to isolate some of the reaction paths. Using the model we have then been able to determine the rates of key reactions in the various paths.

In all of the Ar-Kr- F_2 mixtures the F_2 fraction was 0.1%. The largest Kr fraction in the experiments was 3%. In this case the KrF^* is formed via the dimer-ion recombination channel,



The rate inferred for this reaction from the analy-

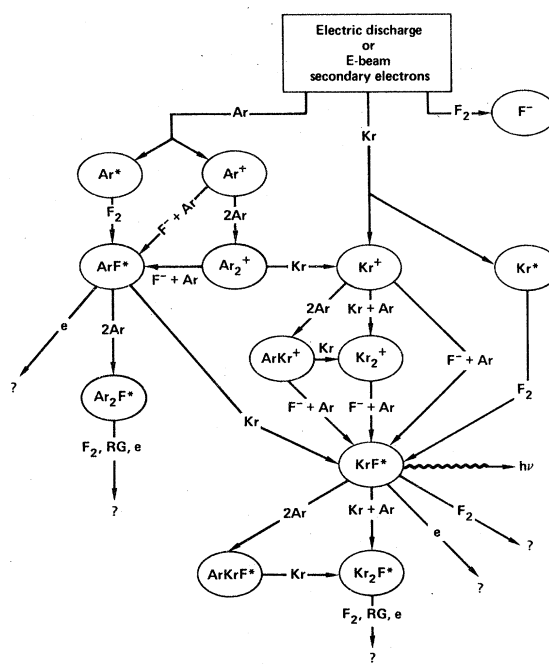
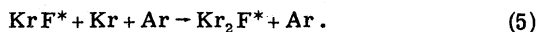


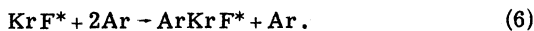
FIG. 6. Schematic kinetic pathways leading to formation of KrF^* and Kr_2F^* in an Ar-Kr- F_2 mixture.

sis of the pressure dependence of KrF* decay rates is 0.7 times the Flannery and Yang³⁶ theoretical rate. The trimer Kr₂F* is formed by



This rate was determined to be 8×10^{-31} cm³/sec based on the pressure dependence of integrated KrF* fluorescence. Typical laser mixtures are composed of 6–9% Kr so that these would be expected to be the dominant formation mechanisms for the Kr-F exciplexes.

For very low Kr fractions, 0.3% in this experiment, KrF* appears to form primarily via ionic recombination of ArKr⁺. This recombination rate is found to be 0.5 times that predicted by the theory of Flannery.³⁵ Calculation of the recombination rate requires the knowledge of the mobility of ArKr⁺ in the Ar buffer. This was computed using the Langevin formula. For low Kr partial pressures the KrF is quenched primarily by the three-body process



Although the existence, not to mention the physical characteristics, of ArKrF* is in question³⁹ it is useful in this model to provide the proper pressure dependences of the KrF* and Kr₂F* integrated signals. The Kr₂F* is produced by Kr replacement in ArKrF*. The rate coefficients inferred for these processes are listed in Table II.

The Stern-Volmer plot in Fig. 7 indicates the role of Ar* and Ar⁺ in the kinetic chain leading, ultimately, to the formation of KrF*. This is a plot of the reciprocal of the integrated ArF* intensity versus krypton partial pressure. The total gas pressure is 1000 Torr. From the dashed line in Fig. 7 we obtain the half quenching pres-

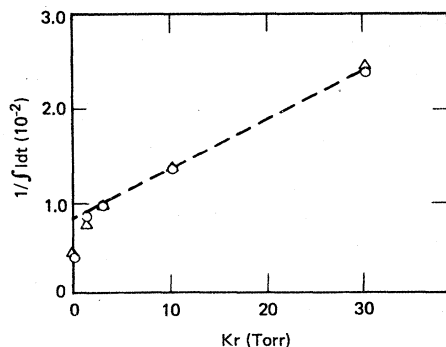


FIG. 7. Stern-Volmer plot of ArF* integrated intensity as a function of Kr partial pressure in a 1000-Torr Ar-Kr-F₂ mixture with 0.1% F₂. Δ —experimental points; \circ —calculated points.

sure. From this we infer a rate coefficient of 3.3×10^{-10} cm³/sec for the displacement reaction

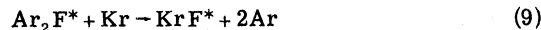


As can be seen in Fig. 6, the calculations and experimental data agree well. The deviation from linearity at low partial pressure is due to the interception of the Ar₂⁺-F⁻ recombination channel by charge transfer between Ar₂⁺ and Kr. The previously measured rate coefficient for this charge transfer is 7.5×10^{-10} cm³/sec,²⁸ which is consistent with our modeling of the ArF* formation kinetics. Because of this, we observe a near exponential decay of the ArF* fluorescence in the experiment at high pressures. Consequently, most ArF* at high Kr partial pressures is formed via the so-called "harpoon" reaction



Our analysis gives a rate coefficient of 4×10^{-10} cm³/sec for this reaction based on the observed ArF* decay rate. This is in agreement with the most recent measurement of Kolts and Setser.³²

We observe from the experimental fluorescence data that the KrF* decay (formation) rate is slower than the ArF* decay (formation) rate. Because of this we postulate the displacement reaction



as another channel for formation of KrF*. Because the analogous displacement reaction for ArF* is relatively slow ($k = 3 \times 10^{-10}$ cm³/sec) the three-body formation of Ar₂F* would be expected to be competitive to moderate pressures. Reaction (9) then provides an efficient means of forming KrF* that makes up for the slowness of reaction (7). This reaction looks structurally very similar to the ionic displacement reaction ($k = 7.5 \times 10^{-10}$ cm³/sec) and would be expected to have a similar rate coefficient. Unfortunately, we have no data on the Ar₂F* fluorescence because it overlaps the KrF* (C-A) band.

As the figures presented above have shown, this model, using the rate coefficient data just discussed, gives excellent agreement with our own experimental data. In Figs. 8 and 9 are shown comparisons between model prediction and other experimental data taken from the literature.^{2,40} In Fig. 8 relative KrF* fluorescent intensity for Ar-Kr-F₂ mixtures containing 0.3% F₂ and 1 and 15% Kr is shown for a variety of pressures between 0.25 and 4.0 atm and an e-beam current density of 10 A/cm². The calculations are normalized to the experimental data at 1% Kr and 1 atm total pressure and, as can be seen, the agreement is excellent over the whole pressure range and for both Kr fractions. Absolute KrF*

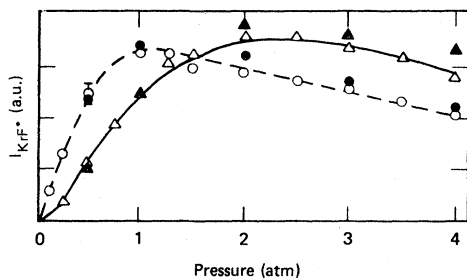


FIG. 8. Relative intensity of KrF^* as a function of pressure and Kr fraction in an Ar-Kr- F_2 mixture with 0.3% F_2 . Δ , \circ —experiments of Mangano *et al.* (Ref. 40) with 1% Kr and 15% Kr, respectively. \blacktriangle , \bullet —calculations using the model presented in this paper.

fluorescence efficiencies are plotted similarly in Fig. 9. Again the agreement is good although the model predicts a somewhat different pressure dependence of the fluorescence efficiency for the larger Kr partial fraction.

V. CONCLUSION

In the preceding section we have presented the results of an experimental and computational effort to determine rate coefficients for some important rare-gas-fluoride kinetic processes. We have assembled a detailed model of the kinetics of e -beam pumped Ar-Kr- F_2 mixtures and have used this model to analyze our experimental fluorescence data. We have also shown that the model gives good agreement with the experimental data of others as well as our own. As a general result we have found the rate coefficients for positive-negative ionic recombination to be slower than predicted by theory. There is further support for this conclusion from the recent Monte-Carlo calculations of Bardsley and Wadehra⁴¹ and of Morgan *et al.*⁴² which also yield lower recombination rates. These classical trajectory calculations avoid some of the less rigorous assump-

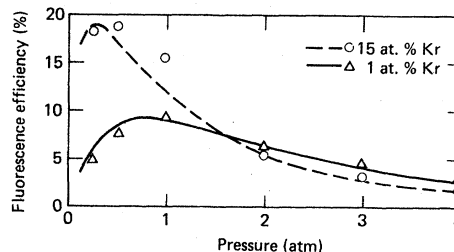


FIG. 9. KrF^* fluorescence efficiency as a function of pressure and Kr fraction for the conditions of Fig. 8. The lines are the experimental curves of Mangano *et al.* (Ref. 40) and the symbols (Δ , \circ) are calculations using the model presented in this paper.

tions, such as the concepts of “trapping radius”, “average” ion pair, and recombination via a single three-body collision, inherent in the available analytic theories of ionic recombination.^{34,35} In addition, the calculations of Morgan *et al.*⁴² include the effects of plasma screening of the interionic potential, which leads to a further reduction in the recombination rate. This results in a reduction in the efficiency that such a model would predict for a KrF^* amplifier. Results from this kinetic model have been used to predict laser amplifier performance.⁴³ In addition, this model used in conjunction with a laser extraction code has given good agreement with experimental data on pulse shape and extraction efficiency from a KrF^* amplifier.⁴⁴ This gives us reason to have confidence in the predictive capabilities of the model presented in this paper.

ACKNOWLEDGMENTS

The authors gratefully acknowledge the technical assistance of R. Wilder and D. Prosnitz in this research. This work was performed under the auspices of the Department of Energy at Lawrence Livermore Laboratory under Contract No. W-7405-Eng-48.

¹M. Rokni, J. H. Jacob, and J. A. Mangano, *Phys. Rev. A* **16**, 2216 (1977).

²M. Rokni, J. A. Mangano, J. H. Jacob, and J. C. Hsia, *J. Quantum Electron.* **14**, 464 (1978).

³M. R. Flannery, *Int. J. Quantum Chem. Symp.* **13**, 501 (1979).

⁴L. S. Frost and A. V. Phelps, *Phys. Rev.* **136**, A1538 (1964).

⁵M. Schaper and H. Scheibner, *Beitr. Plasma Phys.* **9**, 45 (1969).

⁶E. Eggarter, *J. Chem. Phys.* **62**, 833 (1975).

⁷D. Rapp and P. Englander-Golden, *J. Chem. Phys.* **43**, 1464 (1965).

⁸I. P. Zapesochnyi, E. N. Postoi, and I. S. Aleksakhin, *Zh. Eksp. Teor. Fiz.* **68**, 1724 (1975) [*Sov. Phys. JETP* **41**, 865 (1976)].

⁹D. Ton-That and M. R. Flannery, *Phys. Rev. A* **15**, 517 (1977).

¹⁰J. H. Jacob and J. A. Mangano, *Appl. Phys. Lett.* **28**, 724 (1976).

¹¹T. N. Rescigno, C. F. Bender, C. W. McCurdy, and V. McKoy, *J. Phys. B* **9**, 2141 (1976).

¹²T. N. Rescigno, private communication.

¹³R. J. Hall, *J. Chem. Phys.* **68**, 1803 (1978).

¹⁴P. J. Chantry, Attachment Measurements in Halogen Bearing Molecules, Westinghouse R & D Center, final

- Technical Report No. 78-966-ATACH-RI, unpublished.
- ¹⁵A. W. Fliflet, V. McKoy, and T. N. Rescigno, *Phys. Rev. A* **21**, 788 (1980).
- ¹⁶T. N. Rescigno, C. F. Bender, and V. McKoy, *Chem. Phys. Lett.* **45**, 307 (1977).
- ¹⁷L. R. Peterson, *Phys. Rev.* **187**, 105 (1969).
- ¹⁸W. L. Morgan, *A Study of the Plasma Chemistry of the Argon Oxide Laser*, (Wayne State University, Detroit, Michigan); RIES Report No. 75-109 (unpublished).
- ¹⁹A. E. S. Green and T. Sawada, *J. Atmos. Terr. Phys.* **34**, 1719 (1972).
- ²⁰L. R. Peterson and J. E. Allen, Jr., *J. Chem. Phys.* **56**, 6068 (1972).
- ²¹K. J. Nygaard, H. L. Brooks, and S. R. Hunter, *J. Quantum Electron.* **15**, 1216 (1979).
- ²²W. L. Nighan, *J. Quantum Electron.* **19**, 714 (1978).
- ²³R. T. Brown and W. L. Nighan, *Appl. Phys. Lett.* **32**, 142 (1979).
- ²⁴J. Wilson, H. L. Chen, W. Fyfe, and R. L. Taylor, *J. Appl. Phys.* **44**, 5447 (1973).
- ²⁵H. L. Chen, R. E. Center, D. W. Trainor, and W. I. Fyfe, *J. Appl. Phys.* **48**, 2297 (1977).
- ²⁶W. L. Morgan, Joint Institute for Laboratory Astrophysics Information Center Report No. 19 (unpublished).
- ²⁷A. E. S. Green and C. A. Barth, *J. Geophys. Res.* **70**, 1083 (1965).
- ²⁸A. V. Phelps, Ion-Atom Reactions in Rare Gases, Joint Institute for Laboratory Astrophysics Data Memo No. 1 (unpublished).
- ²⁹V. H. Shui and C. Duzy, *Appl. Phys. Lett.* **36**, 135 (1980).
- ³⁰G. P. Quigley and W. M. Hughes, *Appl. Phys. Lett.* **32**, 649 (1978).
- ³¹J. E. Velazco, J. H. Kolts, and D. W. Setser, *J. Chem. Phys.* **65**, 3468 (1976).
- ³²J. H. Kolts and D. W. Setser, *J. Phys. Chem.* **82**, 1766 (1978).
- ³³C. H. Chen and M. G. Payne, *J. Quantum Electron.* **15**, 149 (1979).
- ³⁴D. R. Bates and M. R. Flannery, *J. Phys. B* **2**, 184 (1969).
- ³⁵M. R. Flannery, *Chem. Phys. Lett.* **56**, 143 (1978).
- ³⁶M. R. Flannery and T. P. Yang, *Appl. Phys. Lett.* **33**, 574 (1978).
- ³⁷H. Pummer and K. Hohla, Topical Meeting on Excimer Lasers, Charleston, South Carolina, September, 1979 (unpublished).
- ³⁸P. J. Hay and T. H. Dunning, Jr., *J. Chem. Phys.* **66**, 1306 (1977).
- ³⁹C. H. Chen, M. G. Payne, and J. P. Judish, *J. Chem. Phys.* **69**, 1626 (1978).
- ⁴⁰J. A. Mangano, J. H. Jacob, M. Rokni, and A. Hawryluk, *Appl. Phys. Lett.* **31**, 26 (1977).
- ⁴¹J. N. Bardsley and J. M. Wadehra, *Chem. Phys. Lett.*, **72**, 477 (1980).
- ⁴²W. L. Morgan, B. L. Whitten, and J. N. Bardsley, *Phys. Rev. Lett.* **45**, 2021 (1980).
- ⁴³J. J. Ewing, R. A. Haas, J. C. Swingle, E. V. George, and W. F. Krupke, *J. Quantum Electron.* **15**, 368 (1979).
- ⁴⁴J. C. Swingle, L. Schlitt, R. Rapoport, D. Eimerl, and J. J. Ewing, Topical Meeting on Excimer Lasers Charleston, South Carolina, September, 1979 (unpublished).